Research on hybrid β-energy spectral analysis algorithm based on Fourier series function

Hao Fan[1] · Jun Qin[2] · Bao-Hua Liu[3] · Tin-Xuan Yuan[1] · Wei Zhou[1]

Abstract

With the rapid development of the nuclear power industry on a global scale, the discharge of radioactive effluents from nuclear power plants and their impact on the environment have become important issues in radioactive waste management, radiation protection, and environmental impact assessments. β-detection of nuclides requires tedious processes, such as waiting for the radioactive balance of the sample and pretreatment separation, and there is an urgent need for a method specifically designed for mixing β rapid energy spectrum measurement method for nuclide samples. The analysis of hybrid β-energy spectrum is proposed in this study as a new algorithm, which takes advantage of the spectral analysis of β-logarithmic energy spectrum and fitting ability of Fourier series. The logarithmic energy spectrum is obtained by logarithmic conversion of the hybrid linear energy spectrum. The Fourier fitting interpolation method is used to fit the logarithmic energy spectrum numerically. Next, the interpolation points for the 'effective high-energy window' and 'effective low-energy window' corresponding to the highest E_m nuclide in the hybrid logarithmic fitted energy spectrum are set, and spline interpolation is performed three times to obtain the logarithmic fitted energy spectrum of the highest E_m nuclide. Finally, the logarithmic fitted spectrum of the highest E_m nuclide is subtracted from the hybrid logarithmic fitted spectrum to obtain a logarithmic fitted spectrum comprised of the remaining lower E_m nuclides. The aforementioned process is iterated in a loop to resolve the logarithmic spectra of each nuclide in the original hybrid logarithmic spectra. Then, the radioactivity of E_m nuclides to be measured is calculated. In the experimental tests, ^{14}C, ^{90}Sr, and ^{90}Y spectra, which are obtained using the Fourier fitting interpolation method are compared with the original simulated ^{14}C, ^{90}Sr, and ^{90}Y spectra of GEANT4. The measured liquid scintillator data of ^{90}Sr/^{90}Y sample source and simulated data from GEANT4 are then analyzed. Analysis of the experimental results indicates that the Fourier fitting interpolation method accurately solves ^{14}C, ^{90}Sr, and ^{90}Y energy spectra, which is in good agreement with the original GEANT4 simulation. The error in ^{90}Y activity, calculated using the actual detection efficiency, is less than 10% and less than 5% when using the simulated full-spectrum detection efficiency, satisfying the experimental expectations.

Keywords Nuclear power effluents · Hybrid β energy spectrum · Fourier series · Cubic spline interpolation · Activity calculation

✉ Wei Zhou
8419007@qq.com

1 The College of Nuclear Technology and Automation Engineering, Chengdu University of Technology, Chengdu 610059, China

2 The Engineering Technical College of Chengdu University of Technology, Leshan 614000, China

3 Guangdong Provincial Environmental Radiation Monitoring Center, Guangzhou 510800, China

1 Introduction

The discharge of radioactive effluents [1] from nuclear power plants and their radiological impact on the environment are significant concerns in radioactive waste management, radiation protection, and environmental impact assessment owing to the rapid development of nuclear power generation worldwide [2, 3]. Radioactive fission products are produced in fuel during power generation in nuclear power plants. Neutron activation products are produced in structural and cladding materials. These fission products may be released from the

small amount of fuel in the broken cladding into the reactor coolant, causing radioactive contamination. This results in coolant effluents containing artificial radionuclides, such as ^{90}Sr, ^{137}Cs, and ^{60}Co [4], all of which undergo β decay to produce β rays. ^{90}Sr and its daughter ^{90}Y are pure β decay nuclides and are considered to be highly dangerous radionuclides and carcinogens. Once ^{90}Sr is absorbed by the human body, it is stored in bones and cannot be eliminated. Therefore, it is crucial to locate and quantify ^{90}Sr activity to assess the effects of radiation on nuclear power plant workers. On March 18, 2023, the Japanese government announced that equipment for discharging contaminated water from Fukushima into the sea was in operation [5]. It is expected that over a period of 30 years, more than one million tonnes of nuclear waste will be discharged into the sea. Radioactive substances accumulate in marine food chains over time and pose potential health risks to humans [6–8]. Measuring β-emitting radionuclides in nuclear fuel and radioactive effluents is essential for understanding the activity of the fuel and the radioactive content of the waste. This facilitates the management and disposal of radioactive waste. These spectra exhibit a continuous distribution of particle energies E_β ranging from 0 to E_m (E_m is the maximum energy of a β particle). The analysis of the energy spectra produced by the measurement of β-emitting radionuclides in radioactive effluents can be challenging because of the complex mixture of energy spectra resulting from the combination of several radionuclides [9, 10]. To address these issues, a typical approach involves performing laborious chemical separation of the β-radionuclide mixture, followed by instrumental detection. However, this method increases the time required and generates chemical waste during the separation process, which can lead to harmful effects on the environment [11–13].

Research on spectrum analysis methods for the hybrid β-energy spectrum has been conducted domestically and internationally for many years to simplify the process. In 2016, Gui-Feng et al. proposed a method for analyzing the spectrum by establishing a linear relationship between the fitting parameters and quenching index based on the asymmetric dual sigmoid function fitting of the $^{90}Sr/^{90}Y$ liquid scintillation logarithmic energy spectrum at different quenching levels [14]. In 2022, Castells et al. developed the DECLAB software for analyzing the liquid scintillation β-logarithmic energy spectrum. They constructed a partial least-squares (PLS) model for the standard liquid scintillation β-logarithmic energy spectrum and considered classical calibration models, such as constant efficiency and quenching curves, in a liquid scintillation spectrometer [15]. The aforementioned studies partially resolved the issue of separating samples for measurement. However, they encounter problems such as poor fitting and low measurement efficiency. To overcome these issues, in this study, we propose a new algorithm, the Fourier fitting interpolation method, for resolving hybrid β-energy spectra. This method is based on the spectral analysis advantages of the β-logarithmic energy spectrum and fitting ability of the Fourier series function. It realizes fast and accurate resolution of the hybrid β-energy spectrum data and provides a new method for more efficient β-nuclide measurements.

2 Material and methods

2.1 Material

Figure 1 shows $^{90}Sr/^{90}Y$ sample source used in the activity error analysis, which was prepared by the Guangdong Radiation Environment Monitoring Technology Center. The method for preparing $^{90}Sr/^{90}Y$ sample source was as follows: 10 mL of $^{90}Sr/^{90}Y$ standard equilibrium solution with a reference activity of 37.157 Bq/mL was used. Subsequently, strontium [16] and yttrium [17] carriers were added, and oxalic acid was added to precipitate strontium oxalate and yttrium oxalate. The resulting $^{90}Sr/^{90}Y$ sample source had a 100% recovery rate. The β sample source had an initial activity of 371.44 Bq and was used for the activity error analysis experiments.

2.2 β-logarithmic energy spectrum system

In contrast to the shapes of α and γ decay spectra [18], the β decay spectrum is continuously distributed. Figure 2 shows the β-linear energy spectrum [19]. Given that β nuclides emit βparticles with a continuously distributed energy range from zero to the maximum energy E_m, some β measurement systems use a logarithmic processing function to handle the β energy spectra. Figure 3 illustrates this logarithmic conversion process.

β-Logarithmic energy spectroscopy offers several advantages over linear energy spectroscopy. First, it can significantly enhance the energy resolution in the low-energy range without significantly reducing that in the high-energy range. This solves the problems of inaccuracy and incompleteness
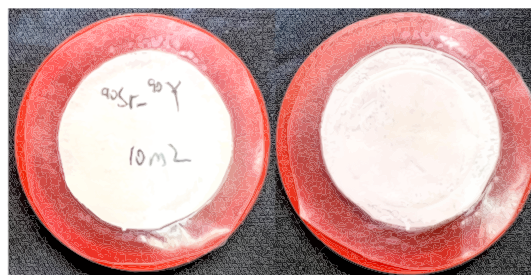

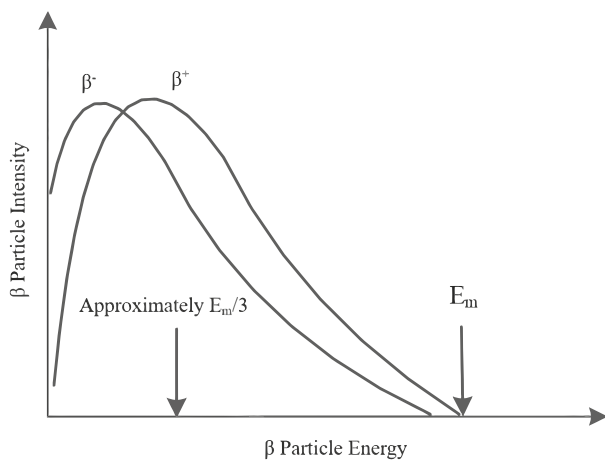**Fig. 1** (Color online) Sample source for $^{90}Sr/^{90}Y$
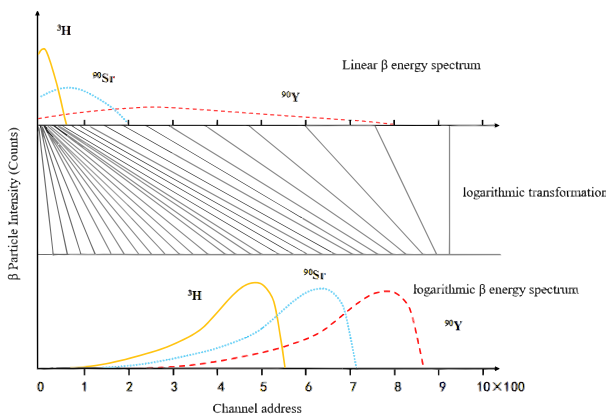
Fig. 2 β-particle energy spectrum

Fig. 3 (Color online) Conversion of β-linear and logarithmic energy spectra

of the linear energy spectrum at the low-energy end of the measurement. When analyzing low-activity decay events, the statistical error for each energy channel remains almost constant across the entire energy range of the measurement, owing to the flat background spectral line of the β-logarithmic energy spectrum. Therefore, liquid scintillation spectrometry [20] logarithmic processing of β energy spectrum is more suitable for conducting energy spectral analyses of two or more β nuclides.

2.3 Fourier series function fitting model

Curve fitting [21] is a widely used technique in data analysis, statistics, and computer vision, among other fields. Its primary objective is to gain a better understanding of the data, make predictions, and infer the underlying laws by constructing mathematical expressions that match data trends.

Common curve fitting methods include the least-squares, kernel, and spline methods [22, 23].

Least squares [24] is a widely adopted curve fitting technique. The core concept involves minimizing the sum of the squares of the residuals between the model predictions and actual observations by adjusting the model parameters. This achieves optimal fitting. In practice, the least-squares method can be used to determine the coefficients of a model. This ensures that the fitted curve closely follows the distribution trend of the real data, thereby improving the accuracy and reliability of the model predictions. However, the least-squares method is highly sensitive to outliers. Therefore, when fitting the hybrid β-energy spectrum, any outliers or noise in the data can significantly affect the fitting results, causing the fitting curve to deviate from the real data trend [25]. Equation 1 shows the least-squares method for a model with n data points: Here, y_i represents the actual data point value and $f(x_i)$ represents the value fitted by the model.

$$\min \sum_{i=1}^{n} (y_i - f(x_i))^2 \tag{1}$$

The kernel method [26] is a technique for curve fitting using locally weighted regression, in which the core idea involves determining the parameters of the model by assigning different weights to each data point based on its nearby neighbors. Using the kernel method, we were able to capture the local characteristics of the data points, thus obtaining more accurate and finer curve fitting results and improving the fitting effect and predictive ability of the model. However, the computational complexity of the kernel method is usually high, particularly when dealing with large-scale data, and the amount of computation can be extremely large, resulting in a lengthy process when fitting a hybrid β-energy spectrum [27]. For a model with n data points, the kernel method is expressed by Eq. 2. Here, y_i denotes the value of the actual data point, and $w_i(x)$ denotes the weight of the data point i.

$$f(x) = \sum_{i=1}^{n} w_i(x) y_i \tag{2}$$

The core concept of the spline method [28] is to make the overall fitting curve more flexible to adapt to changes in the data by decomposing the data interval into several local regions with a simple polynomial function fitted within each region. Through the spline method, we are able to overcome the overfitting or underfitting problems that may occur during the global fitting process and obtain smoother and more natural fitting curves, which improve the robustness and prediction accuracy of the model. However, the spline method fits the data intervals into segments, which may lead to an overfitting problem if the chosen spline order is too high, making the fitted curve too complex and

insufficiently smooth [29]. For a model with n data points, the spline method is expressed as Eq. 3. Here, $p_i(x)$ denotes the multispline of the ith segment and $I_{[x_{i-1}, x_i]}$ denotes the indicator function.

$$f(x) = \sum_{i=1}^{k} P_i(x) I_{[x_{i-1}, x_i]}(x) \qquad (3)$$

In summary, the least-squares, kernel, and spline methods are not suitable for the curve fitting of hybrid β-energy spectra, despite their respective merits. In the hybrid β energy spectrum, the logarithmic energy spectra of different β nuclides are superimposed; however, the contribution of the highest E_m nuclide to the high-energy channel group is separate, which is characteristic of the high-energy section of the hybrid β logarithmic energy spectrum. Thus, the channel group between the highest energy and second-highest energy nuclides in the hybrid β nuclides is defined as the 'effective high-energy window.' According to a priori knowledge, there must be a section of the channel group with zero counting value after the zero channel, and it can be 'considered' that this channel group is contributed by any nuclide (or the highest E_m nuclide) individually, which is a characteristic of the low-energy section of the hybrid β logarithmic energy spectrum. The channel group is defined as the 'effective low-energy window.' To preserve the spectral line characteristics of the high-energy and low-energy segments in the hybrid β-logarithmic energy spectrum and achieve a better fit, we employed the fitting model based on the 'optimized' Fourier series function to curve-fit the hybrid β-logarithmic energy spectrum, resulting in the hybrid β-logarithmic fitted spectrum.

Equation 4 shows the triangular Fourier series [30], which includes the sine and cosine functions. This series is frequently used in spectral analysis to treat unknown bounded nonperiodic functions as periodic functions in a specific region.

$$f(x) = a_0 + \sum_{k=1}^{\infty} (a_k \cos(k\omega x) + b_k \sin(k\omega x)) \qquad (4)$$

By solving coefficients a_k and b_k in the triangular Fourier series, the information of the original discrete data can be described by a function. For the logarithmic spectral data, the 'optimized' Fourier series function is used to build the fitting model shown in Eq. 5. Here, i denotes the channel value and n_{min} and n_{max} denote the start and end channel values of the selected fitting range, respectively. Furthermore, M denotes the width of the selected range of the spectral fitting, as shown in Eq. 6. a, c_i, and $d_1, d_2, d_3, \ldots, d_N$ denotes the coefficients to be determined; k represents the corresponding fitting order of d_k; and N denotes the order of the fit function.

$$f_F(i) = \begin{cases} a + c_i + \sum_{k=1}^{N} d_k \sin\left(\frac{k\pi i}{M}\right) & i \in [n_{min}, n_{max}] \\ 0 & i \notin [n_{min}, n_{max}] \end{cases} \qquad (5)$$

$$M = n_{max} - n_{min} \qquad (6)$$

When selecting the order of the fitting function N, we calculate the better fitting order N_G using the better curve fitting order algorithm. The procedure is as follows:

- **Step 1:** Establish the Fourier series fitting function model with order N of 0 to 50, choose the Bisquare robust nonlinear least-squares method of LM optimization algorithm to complete the function fitting of order 0 to 50 (robust preprocessing reduces the influence of outliers in the fitted data on the fitting results), and calculate a, c_i, and $d_1, d_2, d_3, \ldots, d_N$ [31, 32].
- **Step 2:** Calculate the sum of squares of the differences between all the fitted data and original data of order N from 0 to 50 using Eq. 7, denoted as S_N^2. Here, $f_{F_N}(i)$ and C_i denote the values of the corresponding counts of the channel i in the hybrid β-logarithmic energy spectrum fitted by order N and in the original hybrid β-logarithmic energy spectrum, respectively.
- **Step 3:** Using Eq. 8 penalty function PF_N, calculate the corresponding order N that minimizes the penalty function PF_N from order 0 to 50 as shown in Fig. 4 as the better fitting order N_G.

$$S_N^2 = \sum_{i=n_{min}}^{n_{max}} [f_{F_N}(i) - C_i]^2 \qquad (7)$$
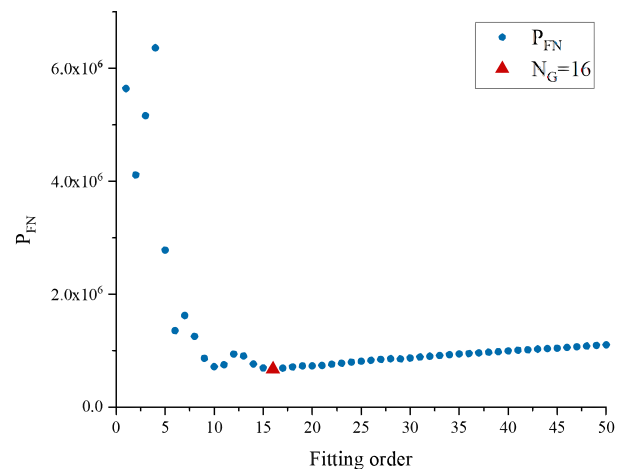
$$PF_N = S_N^2 \sqrt{N} \qquad (8)$$

Fig. 4 (Color online) Penalty function PF_N

$$\min(P_{FN}) \rightarrow N_G \tag{9}$$

The penalty function PF_N is used to measure the quality of the fit, by which it is possible to assess the effectiveness of the fit using different orders and select the fit order that minimizes the penalty function as the better fit order N_G.

If the optimal fitting order N_G does not yield satisfactory results, we can further consider the coefficient of determination R^2 (Eq. 10) corresponding to the fitting function around N_G. By evaluating the distribution of residual values in the 'effective low-energy window' for $i \in [n_{\text{low\_min}}, n_{\text{low\_max}}]$ and the 'effective high-energy window' for $i \in [n_{\text{high\_min}}, n_{\text{high\_max}}]$ regions as well as the smoothness of the curve after fitting, the optimal fitting order N_b can be determined as depicted in Fig. 5. SST (Eq. 11) represents the sum of the squares of the difference between the original data and its mean of the original data. Furthermore, SSR (Eq. 12) represents the sum of the squares of the difference between the fitted data and mean of the original data. C (Eq. 13) represents the average channel count.

$$R^2 = \frac{SSR}{SST} = \frac{SST - S_N^2}{SST} = 1 - \frac{S_N^2}{SST} \tag{10}$$

$$SST = \sum_{i=n_{\text{min}}}^{n_{\text{max}}} [C_i - \overline{C}]^2 \tag{11}$$

$$SSR = \sum_{i=n_{\text{min}}}^{n_{\text{max}}} [f_F(i) - \overline{C}]^2 \tag{12}$$
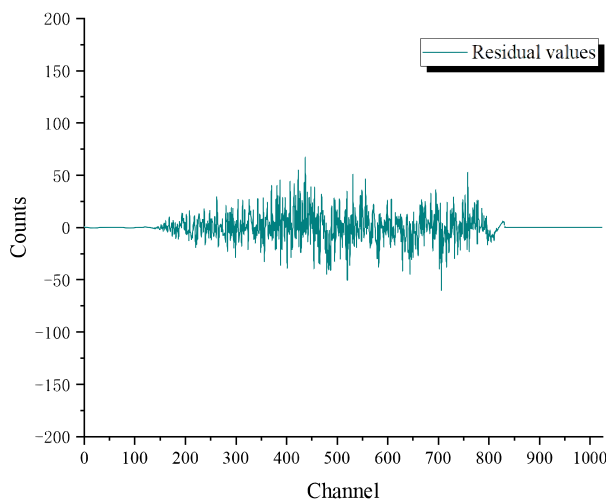
Fig. 5 Distribution of fitted differences

$$\overline{C} = \frac{1}{n_{\text{max}} - n_{\text{min}}} \sum_{i=n_{\text{min}}}^{n_{\text{max}}} C_i \tag{13}$$

Once the order of the optimal fitting function N_b is determined, the hybrid logarithmic fitting energy spectrum can be plotted using $(f_F(i))$ points $i \in [n_{\text{min}}, n_{\text{max}}]$. The 'effective high-energy window' and 'effective low-energy window' can then be set for the highest E_m nuclides in the current hybrid β-logarithmic fitting energy spectrum.

2.4 Cubic spline interpolation

The cubic spline interpolation function [33] 'connects' the 'effective low-energy window' and the 'effective high-energy window' of the hybrid β-logarithmic fitted energy spectrum to produce a smooth continuous curve, i.e., the highest E_m nuclide β-logarithmic fitting energy spectrum. It has the advantages of a simple formula, fast calculation speed, and good stability and is designed to ensure calculation efficiency by making the β-energy spectrum coherent, smooth, and retains the details of the original data in the entire energy range, which provides a more reliable and accurate basis for the subsequent analysis and interpretation of the data [34].

For $y = f(x)$ in a given interval $[a, b]$ with the given p nodes, $a = x_0 < x_1 < \ldots < x_p < b$ and the function values $y_0, y_1, \ldots, y_p$ correspond to the p nodes. Furthermore, $S(x)$ is termed as a cubic spline interpolation function if it satisfies the following conditions:

1. On each subinterval $[x_{k-1}, x_k]$ $(k = 1, 2, \ldots, p)$, $S(x)$ is a polynomial not higher than the third degree;
2. $S(x)$ is second-order derivable in $[a, b]$ interval and the derivative function is continuous, i.e., $S(x) \in C^2[a, b]$;
3. The function $S(x_k)$ is equal to the function value y_k $(k = 1, 2, \ldots, n)$.

From condition (1), $S(x)$ in each $[x_{k-1}, x_k]$ interval can be expressed as Eq. (14):

$$S(x_k) = a_k + b_k x + c_k x^2 + d_k x^3 \quad (k = 1, 2, \ldots, p) \tag{14}$$

To determine the interpolation function in p intervals, $4p$ conditions are required for the $4p$ coefficients to be determined $\{a_k\}, \{b_k\}, \{c_k\}, \{d_k\}$. From condition (2), $S(x)$ should satisfy the conditions shown in Eq. (15) at each node x_k and $3p - 3$.

$$\begin{cases} S^-(x_k) = S^+(x_k) \\ S'^-(x_k) = S'^+(x_k) \quad (k = 1, 2, 3, \ldots, p - 1) \\ S''^-(x_k) = S''^+(x_k) \end{cases} \tag{15}$$

From condition (3) above, $S(x)$ must satisfy all $p + 1$ conditions shown in Eq. (16), and there are already $4p - 2$ conditions in the above statistics.

$$S(x_k) = y_k \quad (k = 0, 1, 2, 3, \ldots, p) \tag{16}$$

Finally, by adding two boundary conditions, $4p$ coefficients and $S(x_k)$ can be determined: The following three boundary conditions are commonly used.

1. Given the values of the first-order derivatives at the two endpoints:

$$\begin{cases} S'(x_0) = z_0 \\ S'(x_p) = z_p \end{cases} \tag{17}$$

2. Given the values of the second-order derivatives at the two endpoints, where it becomes a natural boundary condition when $z_0 = z_p = 0$:

$$\begin{cases} S''(x_0) = z_0 \\ S''(x_p) = z_p \end{cases} \tag{18}$$

$$\begin{cases} S''(x_0) = z_0 = 0 \\ S''(x_p) = z_p = 0 \end{cases} \tag{19}$$

3. $S(x)$ is a function with period $b - a$:

$$\begin{cases} S^-(x_0) = S^+(x_p) \\ S'^-(x_0) = S'^+(x_p) \\ S''^-(x_0) = S''^+(x_p) \end{cases} \tag{20}$$

Specifically, to 'connect' the 'effective low-energy window' and the 'effective high-energy window' using cubic spline interpolation functions, we utilize the fitted spectrum line $f_F(x) = y$ with a given set of p nodes $x_0 < x_1 < \ldots < x_p$ and corresponding function values $y_0, y_1, \ldots, y_p$ as interpolation points within the interval $x \in [n_{low\_min}, n_{low\_max}] \cup [n_{high\_min}, n_{high\_max}]$ [35–37]. This was conducted to perform a cubic spline interpolation. To ensure smoothness and low-count properties at high- and low-energy ends of the hybrid logarithmic fitted energy spectrum, the first-order derivatives, as shown in Eq. (21), are used as boundary conditions in the calculation of the cubic spline interpolation function [38, 39].

$$\begin{cases} S'(x_0) = 0 \\ S'(x_p) = 0 \end{cases} \tag{21}$$

By employing cubic spline interpolation to derive the logarithmic fitting energy spectrum of the highest E_m nuclide in the hybrid logarithmic fitting energy spectrum, the current hybrid logarithmic fitting energy spectrum is subtracted from the logarithmic fitting energy spectrum to yield a logarithmic fitting energy spectrum comprising the remaining lower E_m nuclides. Subsequently, new 'effective low-energy window' and 'effective high-energy window' selections are made in this energy spectrum and inputted into the interpolation analysis process. Iterating through this process allows the resolution of the logarithmic energy spectrum of each nuclide in the original hybrid logarithmic energy spectrum. Finally, activity calculations were performed for each resolved log-fit energy spectrum.

2.5 Algorithmic process

This algorithm has five main modules: logarithmic conversion, curve fitting, cubic spline interpolation processing, difference processing, and activity calculation. The specific process is as follows.

1. Use the logarithmic processing function provided by the liquid scintillation spectrometer to convert the β-linear energy spectrum into a logarithmic energy spectrum;
2. Curve fitting of the hybrid logarithmic energy spectrum using an 'optimized' Fourier series function model with 'effective high-energy windows' and 'effective low-energy windows' for the highest E_m nuclides in the current hybrid β-logarithmic fitted energy spectrum;
3. Select the 'effective high-energy window' and 'effective low-energy window' in the hybrid β log-fit energy spectrum and use cubic spline interpolation to obtain the log-fit energy spectrum of the β nuclide with the highest E_m;
4. Differencing the current hybrid log-fit energy spectrum with the log-fit energy spectrum of the β-nuclide with the highest E_m yields a new hybrid log-fit energy spectrum comprising the other β-nuclides with lower E_m. Substituting this into Step 3 and iterating according to the previous procedure, the logarithmic energy spectrum of each nuclide can be resolved;
5. After resolving the hybrid logarithmic energy spectrum, an activity calculation is performed for each of the resolved logarithmic fitted energy spectra. The activity calculation formula is shown in Eq. 22. Here, A denotes the source activity, C denotes the total counts of the energy spectrum, t denotes measurement time, ε denotes detection efficiency, and R denotes sample recovery rate.

$$A = \frac{C}{t\varepsilon R} \tag{22}$$

3 Results and discussion

The experimental environment involves a liquid scintillation spectrometer and GEANT4 simulation detector model. Two types of experiments were conducted to verify the feasibility and validity of the Fourier fitting interpolation method. First, ^{14}C, ^{90}Sr, and ^{90}Y energy spectra obtained using the Fourier fitting interpolation method were compared with the original simulated ^{14}C, ^{90}Sr, and ^{90}Y energy spectra of GEANT4 to verify the consistency between the measured and simulated energy spectra. Second, the Fourier fitting interpolation method and Asym2Sig method are used to analyze the liquid scintillation test data and GEANT4 simulation data of the ^{90}Sr/^{90}Y sample source, respectively, to evaluate the advantages and limitations of the Fourier fitting interpolation method.

3.1 GEANT4 Simulation of ^{14}C\$^{90}$Sr\$^{90}$Y Energy Spectrum Analysis

The GEANT4 simulated ^{14}C/^{90}Sr/^{90}Y hybrid logarithmic fitted energy spectrum shown in Fig. 6 is fitted using an 'optimized' Fourier series function model. Considering that $E_m = 0.156$ MeV for ^{14}C, 0.546 MeV for ^{90}Sr, and 2.284 MeV for ^{90}Y, the part of the channel group at the high-energy end of the energy interval from 0.546 MeV to 2.2839 MeV (750 to 870 channel group) and the 'presence' section after the zero channel are all counted. Part of the low-energy end of the channel group (channels 0–140), where the counts are all zero, can be considered to be contributed by ^{90}Y with the highest E_m in the mixing spectrum alone. Therefore, the 750 to 870 channel groups and the 0 to 140 channel groups

of the fitted spectra are selected as the 'effective high-energy window' and 'effective low-energy window' corresponding to the highest E_m nuclide ^{90}Y and then they are 'connected' using cubic spline interpolation. Then, using the cubic spline interpolation process, we 'connect' them to obtain a smooth spectrum, i.e., the β-logarithmic fitted spectrum corresponding to the ^{90}Y nuclide.

In the order of E_m from largest to smallest (^{90}Y → ^{90}Sr → ^{14}C), the ^{14}C/^{90}Sr/^{90}Y hybrid log-fit energy spectrum is initially processed by difference with the log-fit energy spectrum of ^{90}Y to obtain the ^{14}C/^{90}Sr hybrid log-fit energy spectrum. Subsequently, ^{14}C/^{90}Sr hybrid log-fit energy spectrum is processed using cubic spline interpolation to obtain a log-fit energy spectrum corresponding to the ^{90}Sr nuclide. Next, the ^{14}C/^{90}Sr hybrid log-fit energy spectrum is processed based on the difference from the log-fit energy spectrum of ^{90}Sr to obtain the ^{14}C log-fit energy spectrum. Finally, ^{14}C/^{90}Sr/^{90}Y log-fit energy spectrum and the resolved ^{14}C, ^{90}Sr, and ^{90}Y log-fit energy spectra were obtained as shown in Fig. 7.

Based on the presentation in Fig. 8, we compared ^{14}C, ^{90}Sr, and ^{90}Y energy spectra, which is obtained by using the Fourier fitting interpolation method with the original GEANT4 simulated energy spectra. The results showed good agreement between the two methods, verifying the feasibility and validity of the Fourier fitting interpolation method in the experimental setting of a liquid scintillation spectrometer. This shows that the energy spectra obtained by the Fourier fitting interpolation method are consistent with the actual simulation data and can accurately reflect the distribution of the particle energy spectra under experimental conditions. This result provides strong support for the use of Fourier fitting interpolation for liquid scintillation spectrometer data analysis and provides a reliable method and
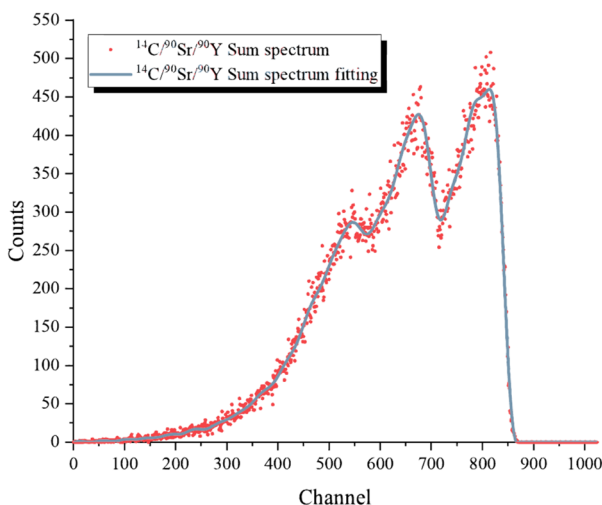

Fig. 6 (Color online) ^{14}C/^{90}Sr/^{90}Y hybrid β-logarithmic fitted energy spectrum

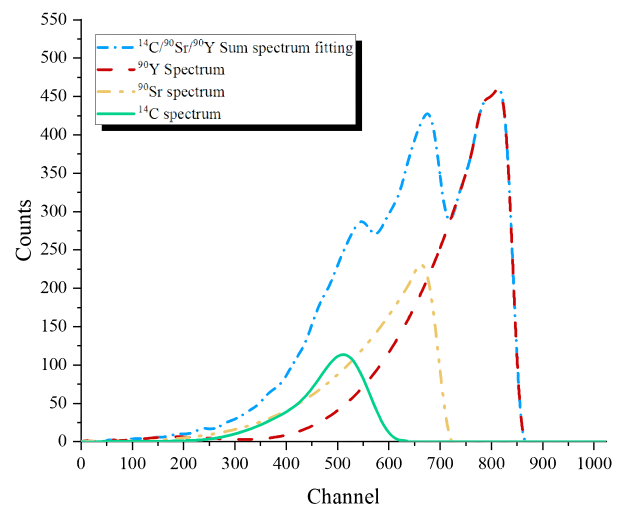**Fig. 7** (Color online) Spectrogram for ^{14}C/^{90}Sr/^{90}Y
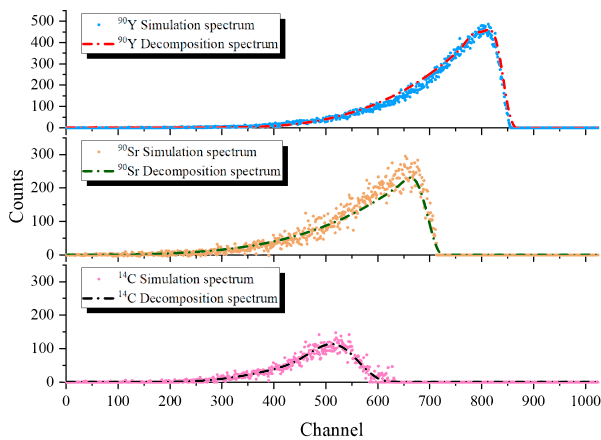
Fig. 8 (Color online) Comparison of ^{14}C/^{90}Sr/^{90}Y logarithmic fitted energy spectral analysis effects

Fig. 9 (Color online) Results of Fourier fitting interpolation analysis of the measured spectra of ^{90}Sr/^{90}Y sample source

basis for the further development of liquid scintillation spectrometers in nuclear physics experiments and applications.

3.2 Activity error analysis

3.2.1 Fourier fitting interpolation method

To measure the ^{90}Sr/^{90}Y sample source, the liquid scintillation spectrometer used was the Quantulus1220 ultra-low-background liquid scintillation spectrometer from Perkin Elmer, USA. The detection efficiencies for ^{3}H and ^{14}C were 25% and 68%, respectively. The background counting rate (relative to the ^{3}H energy region) was 0.067 s^{-1}. The distance between the source and scintillator incident window was set to 1 mm, and the measurement time was 7200 s. The Fourier fitting interpolation method was used to analyze the energy spectrum of the ^{90}Sr/^{90}Y sample source. The results show that the measured detection efficiency of the liquid scintillation spectrometer for the ^{90}Sr/^{90}Y sample source was 25.721%. The full-spectrum detection efficiency of GEANT4 simulation was 27.24%. Given that the initial activity of the ^{90}Sr/^{90}Y sample source is 371.44 Bq and the half-life of ^{90}Y is 64 h, it can be concluded that ^{90}Sr and ^{90}Y in the sample are in a long-term equilibrium state. Therefore, the activities of ^{90}Sr and ^{90}Y are equal, indicating that the actual activity of ^{90}Y is 185.72 Bq.

According to the process described above, the 35th-order 'optimized' Fourier series function is used to fit the measured energy spectrum of ^{90}Sr/^{90}Y and channel group of 340 to 500 is selected as the 'effective high-energy window' corresponding to ^{90}Y. By analyzing the Geant4 simulation results and liquid scintillation energy spectrum data, the corresponding channel of 23.8 keV in the logarithmic energy spectrum of ^{90}Sr/^{90}Y was still in the channel group with a count of zero, and a channel group of 1 to 10 was selected

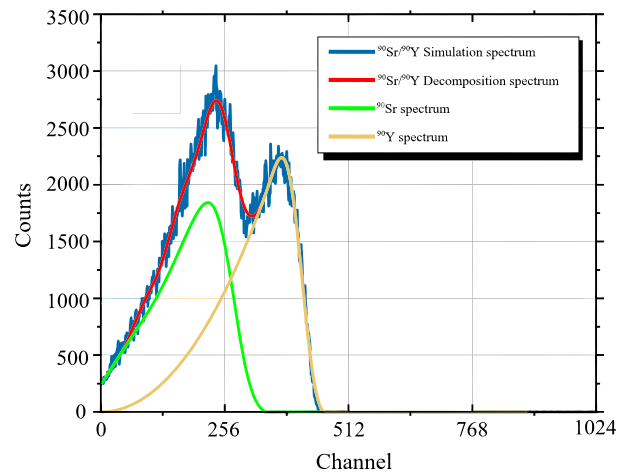as the 'effective low-energy window' of ^{90}Y. Using cubic spline interpolation to 'connect' the 'effective high-energy window' and the 'effective low-energy window' to get a smooth spectrum, i.e., the ^{90}Y energy spectrum. The fitted ^{90}Sr/^{90}Y energy spectrum is subtracted from ^{90}Y energy spectrum to obtain the ^{90}Sr energy spectrum. The results of the Fourier fitting interpolation method for the ^{90}Sr/^{90}Y sample source are shown in Fig. 9.

By analyzing the results of the Fourier fitting interpolation method, we obtain the following conclusions: the average count rate per minute of ^{90}Y is 3173.803 CPM, i.e., the activity of ^{90}Y corresponding to 25.721% of the measured detection efficiency is 205.66 Bq with a relative error of 10.737%; similarly, the activity of ^{90}Y corresponding to 27.24% of the simulated full-spectrum detection efficiency is 194.20 Bq with a relative error of 4.568%. These results are consistent with the test expectations and show that the Fourier fitting interpolation method has a high accuracy and reliability when analyzing the experimental data. These analytical results provide an important reference for the further study and application of the performance of ^{90}Y in liquid scintillation spectrometers, as well as an experimental basis for the optimization and improvement of liquid scintillation spectrometers.

3.2.2 Asym2Sig method

First, an asymmetric double-sigmoid function is used to fit the measured logarithmic energy spectrum data of a pure ^{90}Y sample source. The initial values of the fitting parameters (w_1, w_2, w_3) in the A-term asymmetric double-sigmoid function are determined as 109.9, 74.75, and 12.92, respectively. Based on ^{90}Sr/^{90}Y sample source β, set the peak

count channel locations corresponding to ^{90}Y and ^{90}Sr in the logarithmic energy spectrum and set the initial fitting parameters of the shape parameters (x_c, x_b) to 350 and 180. The asymmetric double-sigmoid function can be obtained as Eq. (24):

$$\delta = \frac{1}{1 + e^{-\left(x - x_c + \frac{w_1}{2}\right)/w_2}},$$

$$\eta = \frac{1}{1 + e^{-\left(x - x_c - \frac{w_1}{2}\right)/w_3}},$$

$$\theta = \frac{1}{1 + e^{-\left(x - x_b + \frac{w_{b1}}{2}\right)/w_{b2}}}, \quad (23)$$

$$\kappa = \frac{1}{1 + e^{-\left(x - x_b - \frac{w_{b1}}{2}\right)/w_{b3}}}$$

$$y(x) = A \cdot (\delta \cdot (1 - \eta)) + B \cdot (\theta \cdot (1 - \kappa)) \quad (24)$$

On this basis, the sum of the asymmetric double-sigmoid functions A and B is used to evaluate ^{90}Sr/^{90}Y β, perform curve fitting on the logarithmic energy spectrum, and determine the final fitted values of 10 shape parameters (A, x_c, w_1, w_2, w_3) and $(B, x_b, w_{b1}, w_{b2}, w_{b3})$ as 3054, 347.8, 110.9, 74.35, 12.92, and 2503, 182.1, 143.8, 56.98, 14.5. Finally, the ten determined shape parameters (A, x_c, w_1, w_2, w_3) and $(B, x_b, w_{b1}, w_{b2}, w_{b3})$ were fed into the single asymmetric double-sigmoid function to obtain the logarithmic energy spectra of ^{90}Sr and ^{90}Y. The energy spectrum analysis results of the Asym2Sig method for the ^{90}Sr/^{90}Y sample source are shown in Fig. 10.

The analysis results of the Asym2Sig method show that the average count rate per minute for ^{90}Y is 3154.871 CPM,
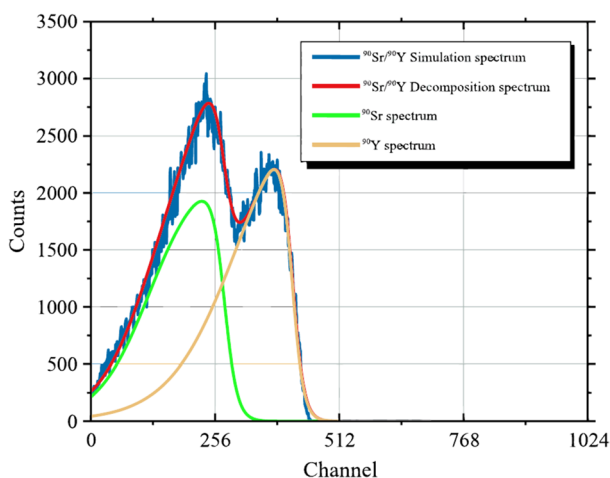

Fig. 10 (Color online) Analysis results of Asym2Sig method for the measured spectrum of ^{90}Sr/^{90}Y sample source

which corresponds to 25.721%. The actual detection efficiency and activity of ^{90}Y are 204.434 Bq with a relative error of 10.077% and ^{90}Y, which corresponds to a simulated full-spectrum detection efficiency of 27.24% with an activity of 193.029 Bq and a relative error of 3.936%, which satisfied the testing expectations.

In summary, the logarithmic energy spectrum analysis results of the measured ^{90}Sr/^{90}Y sample source using the Asym2Sig and Fourier fitting interpolation methods show that ^{90}Y activity errors analyzed by the two spectral-solving algorithms using the actual detection efficiency are both approximately 10%. When using the simulated full-spectrum detection efficiency, the errors are all within 5%, which is in line with experimental expectations. Moreover, the relative error of ^{90}Y activity analyzed using the Asym2Sig method is smaller than that of the Fourier fitting interpolation method, indicating better analysis results. However, given the need to detect pure ^{90}Y sample sources in advance, the analysis using the Asym2Sig method is more cumbersome than that using the Fourier fitting interpolation method. In the actual analysis process, the above two energy spectrum analysis methods can be selected based on the on-site experimental conditions.

4 Conclusion

This research is mainly devoted to the rapid analysis of β nuclides, including ^{14}C, ^{90}Sr, and ^{90}Y, accumulated in the radioactive effluents of nuclear power plants as well as in the surrounding environment. Based on an in-depth understanding of the principle of the measurement and analysis of the logarithmic energy spectrum of β-nuclides, a hybrid β-energy spectrum analysis algorithm, i.e., the Fourier fitting interpolation method, is preliminarily designed and completed. The feasibility and validity of the Fourier fitting interpolation method are verified via two experiments. Firstly, the ^{14}C/^{90}Sr/^{90}Y energy spectra simulated by GEANT4 are analyzed using Fourier fitting interpolation method, and ^{14}C, ^{90}Sr, and ^{90}Y energy spectra obtained by Fourier fitting interpolation method are compared with the original simulated ^{14}C, ^{90}Sr, and ^{90}Y energy spectra of GEANT4. The results showed that the analysis of ^{14}C, ^{90}Sr, and ^{90}Y energy spectra obtained by Fourier fitting interpolation method is in good agreement with the simulated energy spectra of GEANT4. Second, the liquid scintillation measured data and GEANT4 simulated data of ^{90}Sr/^{90}Y sample sources were analyzed using the Fourier fitting interpolation method and Asym2Sig method, respectively. The results showed that when using Fourier fitting interpolation method, the average count rate per minute of ^{90}Y was 3173.803 CPM, which corresponds to an activity of 205.66 Bq at a measured

detection efficiency of 25.721% with a relative error of 10.737%. When using Asym2Sig method, the average count rate per minute of ^{90}Y was 3154.871 CPM, which corresponds to an activity of 204.434 Bq at a measured detection efficiency of 25.721%, with a relative error of 10.077%. When the Asym2Sig method was used, the average count rate per minute of ^{90}Y was 193.029 Bq at a simulated detection efficiency of 27.24%, with a relative error of 3.936%. Therefore, the activity error of ^{90}Y analyzed using the actual detection efficiency of both algorithms was approximately 10%, and the error was within 5% when using the simulated full-spectrum detection efficiency, which is in line with the experimental expectations. Furthermore, the Asym2Sig method had a smaller relative error than the Fourier fitting interpolation method, indicating a better analysis performance. However, Asym2Sig method requires the prior detection of pure ^{90}Y sample sources, making the analysis process more cumbersome than the Fourier fitting interpolation method. Two validation experiments demonstrated the superiority of the Fourier fitting interpolation method. This method not only avoids the cumbersome chemical separation process, but also reduces the harmful effects of chemical waste on the environment. In the future, we will continue to optimize the parameter settings and algorithmic flow of the Fourier fitting interpolation method to improve the accuracy and speed of β-nuclide energy spectra analysis. We introduce additional mathematical models and data processing techniques to address the challenges of applying the algorithm to complex environments such as noise interference and background radiation.

Declarations

References

1. T.Y. Kong, S. Kim, Y. Lee et al., Operating margin for radioactive effluent released to the environment from Korean pressurized water reactors compared to the effluent control limits obtained by monitoring the concentration of radioactive effluent with radioactive effluent monitors. Nucl. Sci. Tech. **56**, 764–769 (2019). https://doi.org/10.1080/00223131.2019.1617205

2. C.N. Danson, M. White, J.R. Barr et al., A history of high-power laser research and development in the United Kingdom. High. Power. Laser. Sci. **9**, 46–131 (2021). https://doi.org/10.1017/hpl.2021.5

3. R.M. Imoru, A.A. Ali, P.N. Bokoro, Analysis of a hybrid nuclear renewable energy resource in a distributed energy system for a rural area in Nigeria. Energies **15**, 7496 (2022). https://doi.org/10.3390/en15207496

4. K. Ogura, M. Hosoda, S. Tokonami, Discriminative measurement of absorbed dose rates in air from natural and artificial radionuclides in Namie Town. Fukushima Prefecture. **18**, 978 (2021). https://doi.org/10.3390/ijerph18030978

5. X. Pan, The application of compulsory conciliation in the settlement of disputes over Fukushima contaminated water discharge. Sci. Prog. **106**, 4 (2023). https://doi.org/10.1177/00368504231191994

6. B.J. Lee, K.B. Jang, T.H. Woo, Analysis of purification in radioactively contaminated ocean water near the Fukushima nuclear accident site. Energy. Sci. Eng. **11**, 3310–3316 (2023). https://doi.org/10.1002/ese3.1538

7. J. Zou, S.C. Liu, C.J. Jin et al., Optimization method of burnable poison based on genetic algorithm andartificial neural network. Ann. Nucl. Energ. **192**, 109985 (2023).https://doi.org/10.1016/j.anucene.2023.109985

8. J. Wang, S.C. Liu, M.C. Li et al., Multiobjective genetic algorithm strategies for burnable poison design of pressurized water reactor. Int. J. Energy Res. **45**, 11930–11942 (2021). https://doi.org/10.1002/er.5926

9. X. Zhang, S.C. Liu, Y.X. Chen, Development of Monte Carlo hybrid parallel algorithm and application in high resolution spatial-energy flux distribution calculation. Elsevier BV **413**, 112500 (2023). https://doi.org/10.1016/j.nucengdes.2023.112500

10. X. Zhang, S.C. Liu, Y.M. Yan et al., Application of the neutron-photon-electron coupling transport of cosRMC in fusion neutronics. Elsevier BV **159**, 111875 (2020). https://doi.org/10.1016/j.fusengdes.2020.111875

11. J.W. Bae, H.R. Kim, In situ beta-gamma separation algorithm for cost-effective assessment of radioactive waste resources. Int. J. Energ. Res. **42**, 4761–4769 (2018). https://doi.org/10.1002/er.4229

12. R. He, X.Y. Niu, Y. Wang et al., Advances in nuclear detection and readout techniques. Nucl. Sci. Tech. **34**, 283–360 (2023). https://doi.org/10.1007/s41365-023-01359-0

13. W. Chen, L. Ma, J.H. Chen et al., Gamma-, neutron-, and muon-induced environmental background simulations for ^{100}Mo-based bolometric double-beta decay experiment at Jinping Underground Laboratory. Nucl. Sci. Tech. **34**, 54–61 (2023). https://doi.org/10.1007/s41365-023-01299-9

14. X.G. Feng, Q.G. He, J.C. Wang et al., A simplified fitting method for liquid scintillation spectra of mixed ^{90}Sr/^{90}Y at different quenching levels. J. Nucl. Radiochem. **38**, 364–370 (2016). https://doi.org/10.7538/hhx.2016.YX.2015041

15. F.C. Jordi, L.B. Inés, F.C. Antonio et al., DECLAB: a software for liquid scintillation spectra deconvolution. J. Radioanal. Nucl. Ch. **331**, 3275–3282 (2022). https://doi.org/10.1007/s10967-022-08365-3

16. C. Daniel, T. Anna, R. Mirjam et al., Determining elemental strontium distribution in rat bones treated with strontium ranelate and strontium citrate using 2D micro-XRF and 3D dual energy K-edge subtraction synchrotron imaging. Xray. Spectrum. **49**, 424–433 (2020). https://doi.org/10.1002/xrs.3127

17. I.A. Afanaseva, V.V. Bobkov, V.V. Gritsyna et al., On the mechanisms of formation of excited yttrium atoms under ion bombardment of yttrium and yttrium-aluminum garnet. Vacuum **129**, 148–152 (2016). https://doi.org/10.1016/j.vacuum.2016.03.014

18. M. Gorchtein, γ^W box inside out: nuclear polarizabilities distort the beta decay spectrum. Phys. Rev. Lett. **123**, 042503 (2019). https://doi.org/10.1103/PhysRevLett.123.042503

19. S.R. Biegalski, AutoCal: a method for automatic energy calibration of β-γ systems based on a ^{137}Cs spectrum. J. Radioanal. Nucl. Chem. **296**, 465–469 (2013). https://doi.org/10.1007/s10967-012-2100-8

20. Y.L. Wu, J.C. Liang, J.C. Liu et al., Standardization of tritium water by TDCR method. Plasma. Sci. Technol. **14**, 644–646 (2012). https://doi.org/10.1088/1009-0630/14/7/17

21. S.S. Li, H.X. Xu, C.Y. Deng, Data-Weighted least square progressive and iterative approximation and related B-Spline curve fitting. Comput. Aided. Des. **31**, 1574–1580 (2019). https://doi.org/10.3724/SP.J.1089.2019.17585

22. H.W. Wu, C. Li, A ROOT-based detector test system. Nucl. Sci. Tech. **32**, 115 (2021). https://doi.org/10.1007/s41365-021-00952-5

23. Z.B. Tang, W.M. Zha, Y.F. Zhang, An experimental review of open heavy flavor and quarkonium production at RHIC. Nucl. Sci. Tech. **31**, 81 (2020). https://doi.org/10.1007/s41365-020-00785-8

24. P.P. Zhang, Q. Wang, Perturbation analysis and condition numbers of mixed least squares-scaled total least squares problem. Numer. Algor. **89**, 1223–1246 (2022). https://doi.org/10.1007/s11075-021-01151-4

25. L.Y. Wang, H. Yu, Study on the applicability of total least squares method in surveying adjustment. Geod. Geodyn. **34**, 121–124 (2014). https://doi.org/10.14075/j.jgg.2014.03.015

26. A. Afkanpour, C. Szepesvári, M. Bowling, Alignment based kernel learning with a continuous set of base kernels. Mach. Learn. **91**, 305–324 (2013). https://doi.org/10.1007/s10994-013-5361-8

27. M.A. Alam, K. Fukumizu, Y.P. Wang, Influence function and robust variant of kernel canonical correlation analysis. Neural. Comput. **304**, 0925–2312 (2018). https://doi.org/10.1016/j.neucom.2018.04.008

28. N. Rajashekar, S. Chaudhary, V.V. Kumar, Approximation of p-Biharmonic problem using WEB-Spline based Mesh-Free method. Int. J. Nonlin. Sci. Num. **20**, 703–712 (2019). https://doi.org/10.1515/ijnsns-2018-0298

29. Y.O. Ala, T.Y. Ying, A.B. Saaban, Quintic spline method for solving Linear and nonlinear boundary value problems. Sains. Malays. **45**, 1007–1012 (2016) https://api.semanticscholar.org/CorpusID:28026763

30. G.A. Karagulyan, K.R. Muradyan, Divergent triangular sums of double trigonometric Fourie series. J. Contemp. Mathemat. Anal. **50**, 196–207 (2015). https://doi.org/10.3103/S1068362315040056

31. J.L. Liang, M.H. Zhang, D. Liu et al., Robust ellipse fitting based on sparse combination of data points. IEEE. T. Image. Process. **22**, 2207–2218 (2013). https://doi.org/10.1109/TIP.2013.2246518

32. C. Hu, C.H. Li, C.Y. Zhang et al., Median robust nonlinear weighted total least squares estimator of nonlinear EIV models: three algorithms. Surv. Rev. **55**, 1–17 (2022). https://doi.org/10.1080/00396265.2022.2127605

33. J.M. Wu, Y.Y. Liu, C.G. Zhu, Integro spline quasi-interpolants and their super convergence. Comp. Appl. Math. **39**, 239 (2020). https://doi.org/10.1007/s40314-020-01286-5

34. P.Z. Li, F.J. Li, X. Li et al., A numerical method for the solutions to nonlinear dynamic systems based on cubic spline interpolation functions. Appl. Math. Mech. **36**, 887–896 (2014). https://doi.org/10.3879/j.issn.1000-0887.2015.08.010

35. K.M. Reddy, N. Vijender, A fractal model for constrained curve and surface interpolation. Eur. Phys. J. Spec. Top. **232**, 1015–1025 (2023). https://doi.org/10.1140/epjs/s11734-023-00862-0

36. H.F. Li, X.L. Shang, W.Z. Chen et al., Fine power reconfiguration calculation of marine reactor core. At. Energy. Sci. Technol. **44**, 307–311 (2010) https://doi.org/CNKI:SUN:YZJS.0.2010-S1-063

37. W.H. Li, X.J. Zhang, Z. Dang et al., Development and preliminary verification of flux map processing software MAPLE. At. Energy. Sci. Technol. **47**, 430–432 (2013). https://doi.org/10.7538/yzk.2013.47.S1.0430

38. I.A. Blatov, A.I. Zadorin, E.V. Kitaeva, Application of cubic splines on bakhvalov meshes in the case of a boundary layer. Comput. Math. Math. Phys. **61**, 1911–1930 (2021). https://doi.org/10.1134/S096554252112006X

39. M. Sun, L. C.G. Lan Wei, Zhu et al., Cubic spline interpolation with optimal end conditions. J. Comput. Appl. Math. **425**, 377–427 (2023). https://doi.org/10.1016/j.cam.2022.115039